1.0

2.8   2.5

1.1   3.2   2.2

3.6

4.0   2.0

1.8

1.25   1.4   1.6

MICROCOPY RESOLUTION TEST CHART
NATIONAL BUREAU OF STANDARDS-1963-A

DAAK 40-77-C-0130

ADA051675

⑮ ⑭ TR-1

② B.S.

⑥ LOW COST LASER GYRO,

PHASE I

④ FINAL REPORT,
on Phase 1,

INERTIAL SYSTEM DEVELOPMENT

GUIDANCE AND CONTROL DIRECTORATE

TECHNOLOGY LAB

⑪ 1978

⑫ 26 p.

U.S. ARMY MISSILE R&D COMMAND

REDSTONE ARSENAL, AL.

⑩ F/Aronowitz, Joseph S. / Killpatrick

F. Aronowitz
Project Engineer

J. Killpatrick
Manager

Honeywell Inc.
Systems & Research Center
2600 Ridgway Parkway
Mpls, Mn. 55433

402 349

TC

TABLE OF CONTENTS

1. INTRODUCTION AND SUMMARY

This contract scope has been planned in two phases. This report summarizes the results of the first phase.

Phase I in the contract was a design study to determine an optimum ring laser gyro size to be used for the Phase II investigations. The criteria to be used in the gyro size evaluation were those applicable to Army missile applications.

As a result of the study, the details of which are presented in this document, a 20 cm path length laser gyro is recommended for the Phase II program. The gyro will be operated with the infra-red transition. The lock-in compensation technique will be an alternating bias obtained by use of the transverse Kerr magneto-optic effect at one of the (magnetic) mirrors.

This size gyro should give sufficient performance margin so that in production, high gyro yield will be compatible with low cost. Reduced size and weight can be obtained by colating three gyros in a common block.

Both a non-rotating and a rotating vehicle have been considered. For the non-rotating case, 100 sec accuracies for a 200 sec mission have been considered. A 100 Hz data bit rate has been considered. All error terms have been shown to decrease with increasing gyro size.

For the rotating case, the 100 sec total error has been shown to put stringent requirements on the scale factor error sources. Hence for a Phase II design, only bias and random drift errors, which are the dominant error source, have been considered.

The suitability of using a low cost laser gyro with a relatively high performance requirement in a short range mission must be further examined. This will be done after the experimental results of the Phase II test program, which will include scale factor tests.

2

2. PERFORMANCE ANALYSIS

2.1 Analysis Assumptions

In this section an error analysis is described which is applicable for the laser gyro mounted onto a non-rolling, slowly rolling and fast rolling vehicle.

The analysis will be applicable only to the laser gyro parameters. Systems and computer generated errors will not be considered.

It will be assumed that a given roll error is allowed. Gyro error will be the cause of this roll error. The various gyro errors will be a function of the mission profile and the gyro design parameters. In the analysis presented here the mission profile will be restricted to the following simple cases.

A short mission time will be assumed. For numerical purposes, a 200 second time will be considered. During this mission time, the gyro will be operated at a constant rotation. For numerical purposes, the three above mentioned cases will be:

   a) non-rolling   zero rate   ;
   b) slowly-rolling   60-300 deg/sec   ;
   c) fast-rolling   300-3600 deg/sec   .

2.2 Analysis Objective

The analysis objective is to determine the effect of various sized gyros on the roll error. The effects of gyro size will enter in various ways. The most obvious is the scale factor. Less direct effects will be numerical values of error parameters such as lock-in threshold and bias stability.

Dither parameters will be considered a variable in the analysis. However, only parameters consistent with the Phase II experimental program will be considered. Hence, the analysis will only treat the case of what will be called square-wave-dither. In this technique, a constant bias is always applied to the laser, irrespective of input rate. During gyro operation, the sense of the bias is rapidly reversed. The reversal rate can be considered a parameter. Hence the bias wave-shape is of the form of a square-wave.

2.3   Error Equation

The basic equation for laser gyro operation is that output counts are obtained which are proportionate to the inertial angle through which the gyro is turned. The equation can be expressed as (time independent parameters assumed)

$$N = S (\theta + \Omega_\beta t), \tag{1}$$

    N :   gyro counts measured in sample time t

    S :   gyro scale factor (cts/$\widehat{sec}$)

    θ :   gyro turning angle ($\widehat{sec}$) during time t

    Ω_β :   gyro bias (deg/hr $\equiv \widehat{sec}$/sec)

The roll error θ_e will be written as

$$\theta_e = \Delta N/S, \tag{2}$$

where ΔN is the experimental data error. Using Equation 1, the data error can be written as

$$\Delta N = \Delta S (\theta + \Omega_\beta t) + S (\Delta \Omega_\beta t + \Delta \theta_q + \Delta \theta_r + \Delta \theta_d) + S \Omega_\beta \Delta t \tag{3}$$

4

ΔS : scale factor error

$\Delta \Omega_\beta$: bias error

$\Delta \theta_q$: quantization error

$\Delta \theta_r$: rms random drift error angle

$\Delta \theta_d$: errors arising from dither mechanization

Δt : clock measurement uncertainty

Using Equations (2) and (3), the roll error can then be written as

$$\theta_e = \frac{\Delta S}{S}(\theta + \Omega_\beta t) + \Delta\Omega_\beta t + \Omega_\beta \Delta t + \Delta\theta + \Delta\theta_q + \Delta\theta_r + \Delta\theta_d \qquad (4)$$

2.4 Case (9) Non-Rolling

The effects of the various errors in Equation (4) will be examined for the case of a non-rolling vehicle. The objective will be to consider the performance potential of various sized gyros.

To check on which are the dominant error sources, an estimate of the accuracy desired must be made. We will consider short mission applications lasting ∼200 sec. An angle error (θ_e) of ∼100 $\widehat{sec}$ will be considered.

Now let us consider the various terms in Equation (4). Since the vehicle is non-rolling, the accumulated angle θ, over the mission, is approximately zero. Hence we have no constraint on the scale factor stability $\Delta S/S$.

The next term is a combination scale factor-bias offset error. Consider an upper bound estimate of this term. For an operational

5

offset of 10 deg/hr over 200 sec, we would get an effective
inertial angle change of 2000 sec. A extremely poor scale factor
stability of 10^3 ppm, would then only give an error of 2 sec.
Hence this term can also be neglected for the non-rolling case.

The next term in Equation (4) is the bias stability error. If
the entire error contribution is from this term, then the bias
stability must be held to 0.5 deg/hr, over the 200 sec. mission.
Hence one of our tasks is to scale bias stability with laser size.
Before considering this, the rest of the terms in Equation (4)
will be examined.

The next term is a time measurement error. This term is negligibly
small for any reasonable time accuracy and will be neglected in all
that follows. Again, it should be noted that we are not considering
system and computer errors.

The next term in Equation (4) is a quantization error. This
term is dependent on the gyro size, the readout mechanization
and the systems computation.

For simplicity, only the simplest readout mechanization is assumed.
For this, we obtain one pulse of output each time our readout
fringe pattern has a phase shift of 2π. Then the gyro quanti-
zation is the angle the gyro must turn to obtain one count of
output. As shown in Appendix A, for an infrared gyro with an
equilateral triangular configuration, the quantization is

$$\frac{1}{S} = K\left(\frac{\overparen{sec}}{ct}\right) = \frac{123}{L\ (cm)} \qquad (5)$$

where L is the laser cavity perimeter.

Thus using Equation (5), we see that for a ten cm path, for example, we get a quantization of 12.3 sec.

The way this quantization affects the error will depend on the systems computation. To proceed with any size analysis, assumptions must be made.

The configuration assumed will be that over the mission of about 200 sec. data counts will be obtained at some sample rate. For analysis purposes, this sample rate will be taken as 100 Hz. Since the output is digital, each data point will contain the gyro quantization error.

It is assumed that the point-to-point data is coherent, so that the quantization error cancels. If the point-to-point data is not coherent, a very large random walk type error can build up. This error can far surpass any other type of error and will not be considered.

With coherent readout, the maximum resultant error due to quantization is just ± 1 count. Thus the quantization error $\Delta\theta_q$ is just

$$\Delta\theta_q = K \qquad\qquad (6)$$

From Equation (5), it can be seen that a larger gyro tends to reduce this error.

The next term in Equation (4) is the RMS random drift error. As discussed in Appendix B, an expression for the RMS random drift error is, for square-wave dither.

$$\Delta\theta_r = \frac{K\,\Omega_L\,(\nu_d t)^{\frac{1}{2}}}{2\,\Omega_d} \qquad\qquad (7)$$

7.

$\Delta\theta_r$: RMS random drift error in $\widehat{sec}$

K : scale factor in $\widehat{sec}$/ct

Ω_L : lock-in threshold in deg/hr

t : time in seconds

ν_d : dither frequency in Hz

Ω_d : dither amplitude in deg/hr

As an illustration of the use of Equation (7) consider a scale factor of 8 $\widehat{sec}$/ct, a lock-in threshold of 5 deg/sec, a dither magnitude of 50 deg/sec and a dither rate of 100 Hz. Then at the end of 200 sec, the RMS random drift error is

$$\Delta\theta_r = 4t^{\frac{1}{2}} = 56 \ \widehat{sec}$$

Note that for this illustration, random drift causes about half the allowable error. Hence, it is one of the critical terms in the gyro design.

The last term in Equation (4) is caused by errors in the dither mechanization. By this we mean errors caused by non-symmetry of the bias. This could be a physical non-symmetry which would result in rectification with an ac bias and a resultant drift. It could also be due to a lack of synchronization between the ac dither and the data dump. This would result in randomness in the output. This randomness however, would not result in a random-walk type error, since it would be bounded.

At the end of the mission, it could however, result in a rather large uncertainty. To see this, consider some randomness between the dither and data dump. Then the maximum error would be just the dither amplitude. As discussed in Appendix B, this is just

8

$$\theta_d = \frac{\Omega_d}{2\nu_d} \qquad\qquad (9)$$

where ϕ_d is the dither amplitude in $\widehat{sec}$, Ω_d is the dither magnitude in deg/hr and ν_d is the dither rate in Hz.

For the previous case of a dither magnitude of 50 deg/sec at 100 Hz, Equation (9) gives

$$\phi_d = \frac{50 \times 3600}{2 \times 100} \equiv 900 \ \widehat{sec} \qquad\qquad (10)$$

Hence it is necessary that in any implementation, care must be taken to insure that lack of dither synchronization does not lead to a large error.

2.4.1   Numerical Evaluation of Error Terms

For the non-rolling case, the roll error equation, given by Equation (4), can be simplified to

$$\theta_e = \Delta\Omega_\beta t + \Delta\theta_q + \Delta\theta_r + \Delta\theta_d \qquad\qquad (11)$$

In using Equation (11), all angles will be expressed in $\widehat{sec}$ and all rates in deg/hr (=$\widehat{sec}$/sec), and all lengths in cm.

In terms of cavity size, short term bias stability for a IR laser can be expressed as

$$\Delta\theta_q = \frac{1.87 \times 10^3 \rightarrow 1.87 \times 10^4}{L^{3.3}} \qquad\qquad (12)$$

The quantization scaling is

$$\Delta\theta_q = \frac{123}{L} \qquad\qquad (13)$$

9

Equation (7) gives an expression for the random drift error $\Delta\theta_r$. The scaling for the lock-in threshold can be written as

$$\Omega_L = \frac{8.26 \times 10^6}{L^{9/4}} \qquad (14)$$

From Equation (5) in Appendix C, the scaling factor for the dither magnitude can be expressed as

$$\Omega_d = \frac{3.29 \times 10^6}{L} \qquad (15)$$

For a dither rate of $\nu_d = 100$ Hz and using Equations (14) and (15) and Equation (13) for the quantization scaling, Equation (7) becomes

$$\Delta\theta_r = \frac{1.54 \times 10^3 t^{\frac{1}{2}}}{L^{9/4}} \qquad (16)$$

To find $\Delta\theta_d$, the dither synchronization error, it will be assumed that a fraction f of the counts occurring during each dither half-cycle are in error. However, if the synchronization circuit is properly designed, this fraction can be made negligably small. For the purposes of size optimization, this will be assumed and $\Delta\phi_d$ will be neglected.

Using Equations (12), (13), and (16), Equation (11) for the roll error becomes

$$\theta_e = \frac{f \times 1.87 \times 10^4 t}{L^{3.3}} + \frac{123}{L} + \frac{1.54 \times 10^3 t^{\frac{1}{2}}}{L^{9/4}} \quad .1 \le f \le 1 \qquad (17)$$

For a mission time of 200 sec, Equation (17) becomes

$$\theta_e = \frac{f \times 3.74 \times 10^6}{L^{3.3}} + \frac{123}{L} + \frac{2.18 \times 10^4}{L^{9/4}} \qquad .1 \le f \le 1 \qquad (18)$$

10

2.4.2   Cavity Optimization

The evaluation of Equation (18) is shown in Figure 1, which describes the roll error as a function of the cavity length. The partial contribution of the individual terms is also shown.

It can be seen that increasing cavity length results in a smaller error for all the error sources. The quantization error is the smallest error source by far, except for larger sized gyros.

Using the 100 sec total error as our criteria, the random drift gives less than half the allowable error for gyros larger than 15 cm path length. The random drift error increases rapidly as the path length decreases past the 15 cm value.

To determine the error contribution due to the drift instability, an estimate of the drift instability for the various gyro sizes has been made. This estimate is given by Equation (12). A plot of Equation (12) is shown in Figure 2. It shows upper and lower estimates of the drift stability of various sized IR gyros.

Honeywell has constructed 10, 20 and 40 cm path length IR gyros, and these curves were obtained as a result of experimental data.

The roll error for the range of drift instabilities are shown in Figure 1. Looking at the lower bound curve, it can be seen that, again, half the allowable error is obtained for a 15 cm path gyro.

At this point in time, it is believed that it would be better to allow some error tolerance by choosing a larger sized gyro. For this reason, the conclusion arived at from the results of the analysis summarized in Figure 1, indicate that a 20 cm perimeter would be an optimum size.
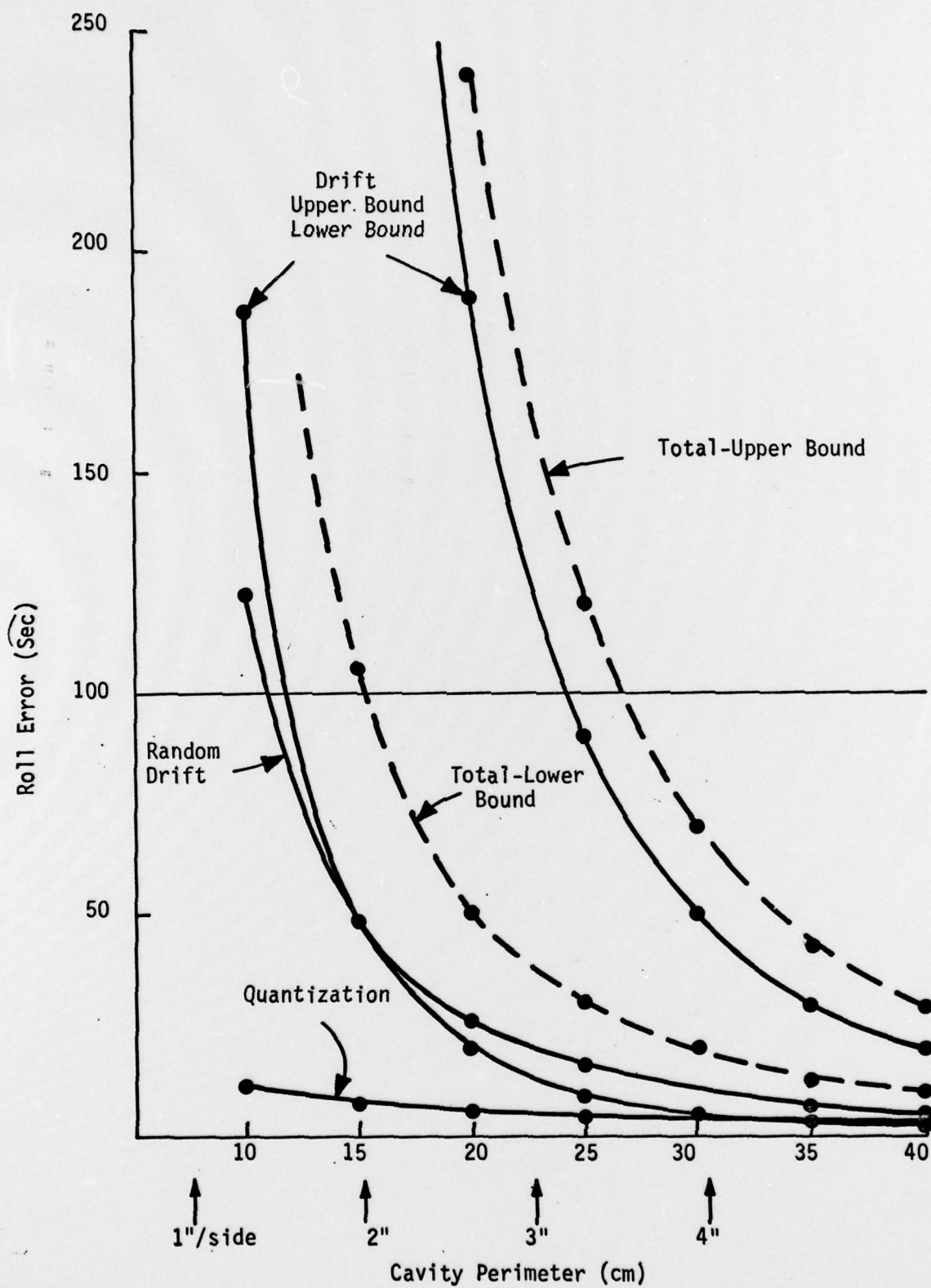
11

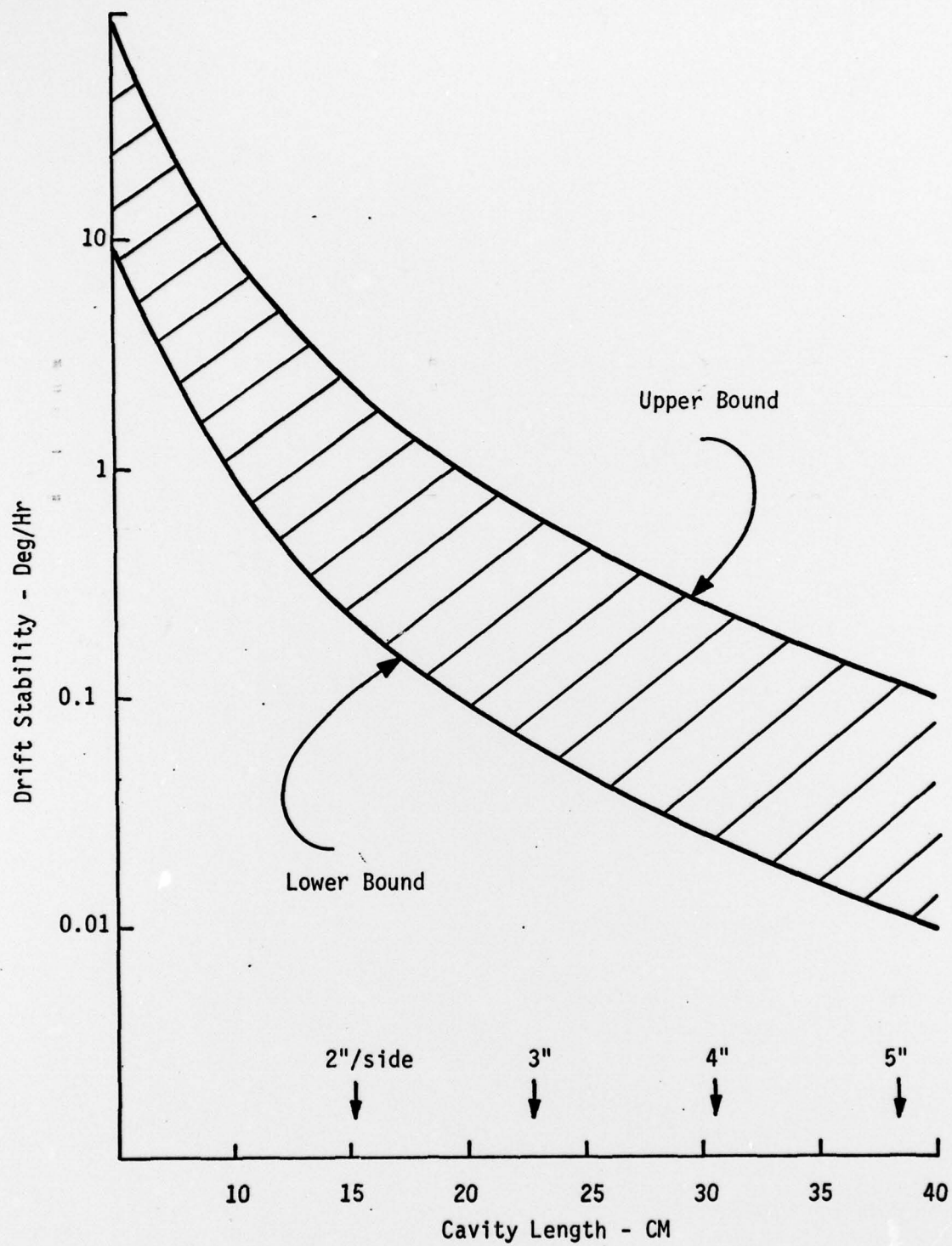Figure 1. Cavity Optimization for Non-Rolling Vehicle

12

Figure 2.   Drift Stability vs Cavity Size

13

2.5   Case(s) - Slowly Rolling

The error analysis obtained for the no-rolling case will now be repeated for the case of a strap-down laser gyro mounted in a slowly rolling vehicle. By slowly rolling, we mean rates in the range of 60-300 deg/sec.

The roll error, described by Equation (18) will still hold for errors due to quantization, drift instability and random drift. We must now include the scale factor error term that was previously neglected. This is the first term in Equation (4).

An upper bound estimate of the scale factor stability that we are interested in can be obtained by writing

$$\frac{\Delta s}{s} \theta < 100 \; \widehat{sec} \tag{19}$$

At the upper rate, assumed constant over the 200 sec. mission, the gyro is turned through an angle

$$\theta = 300 \; \frac{deg}{sec} \times 200 \; sec \times 3600 \; \widehat{\frac{sec}{deg}} = 2.16 \times 10^8 \; \widehat{sec} \tag{20}$$

Thus we see that

$$\frac{\Delta s}{s} < .46 \times 10^{-6} \tag{21}$$

This type of scale factor accuracy is not out of the question, but it is not a trivial problem.

Accuracies of this magnitude are currently being considered by Honeywell for re-entry vehicle applications. However low cost is not a prime consideration for gyros suitable for this type of application.

14

The analysis of the scale factor errors is complicated and is beyond the scope of this first error analysis. This is because the purpose of the analysis is to determine an optimum cavity length to be used for the Phase II part of the program. In this light the errors will be minimized strictly for the non-rotating case.

2.6 Case (C) - Fast Rolling

For the fast rolling case, the scale factor error will be the dominant error source. The discussion in Section 2.5 is even more appropriate here.

3. SKEWED INPUT AXIS

In the discussion presented here, only gyro error sources are considered. Errors due to system algorithms are not considered.

In the non-rolling case, the orientation of the individual gyro axis is immaterial. The input axis stability is the important consideration.

The situation changes for the case of a rolling vehicle. As discussed in Section 2.5, for a rolling vehicle, the scale factor stability becomes a critical issue. To minimize the effect of the scale factor variations, it is desirable to minimize the roll angle. If one of the gyros is along the roll axis, it will receive a maximum roll angle and the scale factor stability requirement will be most stringent.

In this case, however, the other two orthogonal gyros will not receive any appreciable roll angle. Hence, scale factor stability will not be a consideration for these two gyros. This approach implies a higher performance gyro along the roll axis and two lower lower performance gyros in the other two axis. This tends to go in the opposite direction of commonality and low cost and is not recommended.

15

A second approach is to skew all three orthogonally mounted gyros with respect to the roll axis. Then each gyro will see an equal roll rate component which will be about a factor of two lower than the roll rate. Hence by skewing, we can reduce the scale factor requirements by a factor of two. The improvement may not be real, depending on the system algorithm errors.

4. COMMON SOLID BLOCK

One of the advantages in using a magnetic mirror as a laser gyro bias mechanism, is the size reduction it offers. By colating the paths, it is possible, for a given size gyro, to reduce the overall outer dimensions of the gyro package.

A detailed design layout is beyond the scope of this study. It can be stated however, that one of the eventual objectives of this program is to demonstrate the feasibility of constructing a three-axis magnetic mirror laser gyro in a single solid block structure.

Appendix A

Gyro Quantization

This section shows the scaling of the quantization with gyro size. A basic readout mechanism is assumed. By this we mean that a digital readout exists and a single pulse occurs each time one fringe pattern moves across the detector.

The basic laser gyro equation for the beat frequency ($\Delta\nu$), in Hz is

$$\Delta\nu = \frac{4A\Omega}{L\,\lambda} \tag{1}$$

    A - enclosed oven

    L - optical path

    λ - laser wavelength

    Ω - rotation rate (rad/sec)

For an equilateral triangular configuration,

$$A = \frac{\sqrt{3}}{36}\,L^2 \tag{2}$$

Substituting Equation (2) into Equation (1) and integrating with respect to time, we get

$$N = \frac{\sqrt{3}}{9}\,\frac{L}{\lambda}\,\theta \tag{3}$$

where N represents the counts obtained as the gyro turns through θ radian.

The scale factor, expressed in $\overset{\frown}{\text{sec}}$/ct, is then

$$K = \frac{2.06 \times 10^5 \times 9\,\lambda}{\sqrt{3}\,L} = 1.07 \times 10^6 \left(\frac{\lambda}{L}\right) \tag{4}$$

17

Since we are only considering the infrared transition ($\lambda = 1.15 \times 10^{-4}$ cm) Equation (4) becomes

$$K \ (sec/ct) = \frac{123}{L(cm)} \qquad\qquad (5)$$

18

Appendix B

Random Drift

Honeywell has analytically investigated the random drift errors occuring when the gyro is operated with an alternating dither. The analysis is valid for the laser gyro being mechanically dithered with sine wave dither or operated with square wave dither. The square wave dither can be implemented with a magnetic mirror, or any other technique.

For illustrative purposes, first consider sine wave dither. The RMS angle error build up occurs as a random walk phenomena and can be expressed as

$$\theta_r = \frac{K^{\frac{1}{2}} \, \Omega_L \, t^{\frac{1}{2}}}{(2\pi\Omega_D)^{\frac{1}{2}}} \tag{1}$$

θ_r — RMS angle error in $\widehat{sec}$

K — scale factor in $\widehat{sec}$/ct

Ω_L — lock-in threshold in deg/hr

t — time in sec

Ω_D — peak dither rate in deg/hr

To see how Equation (1) is used, consider the Honeywell GG1328 laser gyro operated with, as an example, the following parameters. A lock-in of 720 deg/hr; a dither of ± 200 $\widehat{sec}$ at 500 Hz. The scale factor is 3.14 $\widehat{sec}$/ct.

The dither motion can be written as

$$\phi = \phi_d \sin w_d t \qquad \phi_d = 200 \ \widehat{sec} \tag{2}$$
$$W_d = 2\pi \times 500 \ Hz$$

19

The dither rate is then

$$\dot{\phi} = W_d \, \phi_d \, \cos w_o t \tag{3}$$

The peak dither is then

$$\Omega_d = 2\pi \times 500 \text{ sec}^{-1} \times 200 \, \widehat{\text{sec}} \tag{4}$$

$$= 2\pi \times 10^5 \text{ deg/hr}$$

Equation (1) then becomes

$$\theta_r = \frac{\pi^{\frac{1}{2}} \times 720 \, t^{\frac{1}{2}}}{(2\pi)^{\frac{1}{2}} \times (2\pi \times 10^5)^{\frac{1}{2}}} \approx 0.64 \, t^{\frac{1}{2}} \tag{5}$$

Thus, at the end of 200 sec, the RMS random drift angle error would be 9 $\widehat{\text{sec}}$.

Now consider the same gyro dithered with a square-wave of the same parameters; an amplitude of $\pm$ 200 $\widehat{\text{sec}}$ reversed at 500 Hz.

Then the expression for random drift, corresponding to Equation (1) is

$$\theta_{rs} = \frac{K \, \Omega_L \, t^{\frac{1}{2}}}{4 \, \phi_d \, \sqrt{\nu_d}} \tag{6}$$

θ_{rs} - square wave RMS angle error in $\widehat{\text{sec}}$

K - scale factor in $\widehat{\text{sec}}$/ct

Ω_L - lock-in threshold in deg/hr

θ_d - maximum dither amplitude in $\widehat{\text{sec}}$

ν_d - dither frequency in Hz

20

For the square-wave case, Equation (6) gives

$$\theta_{rs} = \frac{\pi \times 720 \times t^{\frac{1}{2}}}{4 \times 200 \times 500^{\frac{1}{2}}} = 0.13 \; t^{\frac{1}{2}} \qquad (7)$$

Thus at the end of 200 sec, the RMS random drift error would be 1.8 $\widehat{\text{sec}}$. This is a factor of 5 improvement over sine-wave dither.

Comparing Equations (1) and (6), we see that the ratio of RMS random drift error of a square-wave/sine-wave is

$$R = \frac{K \; \Omega_L \; t^{\frac{1}{2}}}{4 \; \phi_d \; \sqrt{\nu_d}} \bigg/ \frac{K^{\frac{1}{2}} \; \Omega_L \; t^{\frac{1}{2}}}{(2\pi)^{\frac{1}{2}} \; (2\pi \; \phi_d \; \nu_d)^{\frac{1}{2}}}$$

$$R = \frac{\pi \; K^{\frac{1}{2}}}{2 \; (\phi_d)^{\frac{1}{2}}} = \frac{\pi}{2} \; \frac{1}{C_d} \qquad (8)$$

where C_d is the dither amplitude in counts

Note that, in agreement with the previous calculations,

$$R = \left(\frac{\pi}{2}\right) \frac{1}{\sqrt{200/\pi}} = .2$$

It is sometimes more convenient to express the random drift given by Equation (6), in terms of dither rate and dither magnitude. The dither amplitude can be written as

$$\phi_d = \Omega_d \; \frac{T_d}{2} = \frac{\Omega_d}{2\nu_d} \qquad (9)$$

where T_d is the dither period in seconds and Ω_d is the dither magnitude in deg/hr.

Using Equation (9), Equation (6) can be written as

$$\theta_r = \frac{K \; \Omega_L \; (\nu_d \; t)^{\frac{1}{2}}}{2 \; \Omega_d} \qquad (10)$$

21

Appendix C

Scaling of Magnetic Bias With Cavity Size

The transverse Kerr Magneto-optic effect is used to obtain a bias.
Physically, the bias is due to a differential phase shift $\Delta\theta$, between
the oppositely directed traveling-waves, that occurs upon reflection at
the "magnetic-mirror". This differential phase shift gives rise to a
best frequency bias, given by

$$\Delta\nu = \frac{C}{L} \frac{\Delta\theta}{2\pi} \tag{1}$$

From eqs. (1) and (2) in Appendix A, this bias is equivalent to an input
rotation Ω_B, which, for an equivalent transverse cavity, is given by

$$\Delta\nu = \frac{L \, \Omega_d}{3 \sqrt{3} \, \lambda} \tag{2}$$

Equations eqs. (1) and (2), we find

$$\Omega_d = \frac{3 \sqrt{3}}{2\pi} \frac{C\lambda}{L^2} \Delta\theta \tag{3}$$

Equation (3) states that for all parameters remaining equal, the magnetic
bias scales inversely with the square of the cavity parameter. Thus, for
small size cavities, where we have larger lock-in thresholds, we get com-
pensation due to the availability of an increased bias magnitude.

There is a question however, on the validity of the assumption of "all
parameters be kept constant". For example, as we increase the cavity size,
we have more available gain. To maintain a constant gain/loss ratio for a
constant laser cavity design, we are at liberty to correspondively increase
the cavity losses. We may do this by increasing the transmission of the
dielectric coating over the magnetic film. Hence, we will get more
light striking the magnetic layer which will result in a larger differential
phase shift.

To take this into account, we can approximately scale the differential
phase shift with path length. Equation (3) can then be written as

$$\Omega_d = {}^a\!/_L \tag{4}$$

22

The constant can be determined emperically. We have obtained a magnetic bias of 60 deg/sec with a 15.24 cm path length IR laser gyro. Thus Eq. (4) can be expressed as

$$\Omega_d = \frac{3.29 \times 10^6}{L} \tag{5}$$

when Ω_d is the magnetic bias in deg/hr and L is the laser cavity path length in cm.